

See discussions, stats, and author profiles for this publication at: <https://www.researchgate.net/publication/231646220>

Study of the Interaction between Silica Surfaces and the Carbon Dioxide Molecule

ARTICLE *in* THE JOURNAL OF PHYSICAL CHEMISTRY C · SEPTEMBER 2010

Impact Factor: 4.77 · DOI: 10.1021/jp107754g

CITATIONS

32

READS

55

3 AUTHORS, INCLUDING:



Rolando M. A. Roque-Malherbe

Materials for Art and Science Use

259 PUBLICATIONS 766 CITATIONS

[SEE PROFILE](#)



Francisco Manuel Marquez

Universidad del Turabo

133 PUBLICATIONS 1,575 CITATIONS

[SEE PROFILE](#)

Study of the Interaction between Silica Surfaces and the Carbon Dioxide Molecule

R. Roque-Malherbe,* R. Polanco-Estrella, and F. Marquez-Linares

Institute for Physical Chemical Applied Research, School of Science, University of Turabo,
P.O. Box 3030, Gurabo, Puerto Rico, 00778-3030

Received: July 6, 2010

Three sphere packing (SP) and three particle packing (PP) silica xerogels, two silica aerogels (AERs), one all-silica mesoporous molecular sieve (MMS), one all-silica molecular sieve (MS), two high Si/Al relation molecular sieves, and an extremely high Si/Al relation molecular sieve were carefully studied with SEM, TGA, SAXS, DRIFTS, and adsorption of nitrogen at 77 K and carbon dioxide at 273 K. The study of different amorphous, ordered, and crystalline silicas, applying numerous powerful and complementary experimental methods and a proper theoretical methodology, is, by itself, an original approach that allows the recognition of the similar features exhibited by the surface of these materials. With the help of SEM, TGA, SAXS, and DRIFTS, it was found that the SP, PP, and AER samples present a complicated pore size distribution composed of micropores and mesopores formed by the agglomeration of primary nanoparticles. The specific surface areas of the synthesized PP silica and one of the AER are extremely high, a fact very significant for the application of these materials as catalyst supports and adsorbents. The specific surface area of the amorphous materials was confirmed with a novel methodology, applying the TGA data. The carbon dioxide adsorption data allowed the measurement of the isosteric heat of adsorption with a single isotherm, applying an original methodology. The contribution of the dispersive interactions to the adsorption energy was theoretically calculated to analyze the separate contribution of the dispersive and the quadrupole interactions. Additionally, the careful analysis of the DRIFT spectra of carbon dioxide adsorbed on silica at 298 K generated information about the carbon dioxide–silica interactions, which allowed us to conclude that, in this interaction, besides the dispersive and quadrupole interactions, there is present a weakly bonded adduct, that is, $H^{\delta+} \cdots O^{\delta-} = C=O^{\delta-}$. This is a new finding as far as we know.

1. Introduction

Adsorption is not only a very important industrial process but also a powerful methodology for the characterization of the surface of materials.^{1–10} In the research reported here, both aspects will be emphasized.

We have studied the interaction of carbon dioxide with the surface of a group of well-characterized porous, amorphous, ordered, and crystalline silica, with the help of different complementary research methods and an appropriate theoretical methodology. This line of attack is unusual because normally these materials are separately studied. It was then possible to identify common and dissimilar characteristics of the surfaces of these materials.

Porous silicas are very important materials in different fields because they are profusely applied as adsorbents, catalyst supports, for membrane preparation, and other large surface and porosity related applications.^{9–12} The molecular properties of silica are strongly affected by the nature of their surface sites. In sol–gel synthesized porous silica surfaces, that is, those of interest here, the unsaturated surface valences are satisfied by surface hydroxyl functionalities, which, depending on the calcination temperature, exists as (a) vicinal (hydrogen-bonded silanols), (b) geminal (two hydroxyl groups attached to the same silicon atom), or (c) isolated (no hydrogen bonds possible) silanol sites.^{7,11}

Adsorption on nanoporous materials is an excellent process for the separation and recovery of gases.^{13–21} The separation and recovery of carbon dioxide is, in particular, a very important research problem because it is a greenhouse gas that contributes to global warming and a reactant in significant industrial processes as, for example, in the Solvay process for the production of NaHCO₃.^{13,14,16,17,22} In this regard, independent of the fact that carbonaceous adsorbents, molecular sieves, alumina, or silica gel can be applied for carbon dioxide separation, applying the pressure swing adsorption (PSA) process, activated alumina is currently considered the most suitable sorbent for removing carbon dioxide from air in a PSA process.^{13,23} Nevertheless, modified silica materials, with a high specific surface area, are currently widely studied as carbon dioxide adsorbents. Particularly, the impregnation of amines in silica is a flourishing field of research.^{14,15,19,24–32} However, these amines are not stable at high temperature, given that these organic substances, on the surface, begin to decompose at about 200 °C.³³ Consequently, another form of modification of silica, by loading oxides^{33–35} in the silica surface, is in development because carbon dioxide will strongly interact with the formed Lewis centers.³⁶

So far, we have described the importance of silica as a porous material and the role of adsorption on modified silica as a separation unitary operation for carbon dioxide production and recovery. Now, we will describe the application of carbon dioxide adsorption as a methodology for the study of the surface of materials.^{37–55} One important application of carbon dioxide adsorption as a characterization tool is for the measurement of the micropore volume and the pore size distribution of nanop-

* To whom correspondence should be addressed. E-mail: RRoquemalh@aol.com. Phone: 1-787-743-7979, ext. 4260. Fax: 1-787-743-7979, ext. 4114.

rous materials.^{50–55} Usually, these measurements are carried out with the help of nitrogen adsorption isotherms measured at 77 K.^{3,9,12,53–55} However, at such a low temperature, the transport kinetics of the nitrogen molecules through the micropores is very slow^{50–52} in pores smaller than 0.7 nm.⁵⁶ In the case of carbon dioxide adsorption, at 273 K, the higher temperature of adsorption applied causes the carbon dioxide molecules to have a bigger kinetic energy; subsequently, they are capable of going into the microporosity for pores of sizes less than 0.7 nm.^{50,51} Therefore, an experimental solution for this difficulty is the use of carbon dioxide adsorption at 273 K instead of nitrogen at 77 K, in order to apply the Dubinin adsorption isotherm to describe carbon dioxide adsorption and calculate the correspondent adsorption parameters.^{57–64} Another significant application of carbon dioxide adsorption as a means for the characterization of the surface chemistry of adsorbents is the study of the infrared spectra of adsorbed carbon dioxide because it is a small weakly interacting probe molecule very useful for the study of the acids and basic properties of solid surfaces.^{37–49}

In the present paper, we report the study of carbon dioxide adsorption interactions in very well characterized amorphous silica: specifically, three sphere packing (SP) silica xerogels,^{65–68} three extremely high specific surface area particle packing (PP) silica xerogels⁶⁹ (these materials were produced with the help of a modification of the Stöber–Fink–Bohm methodology,⁶⁵ i.e., the change of ammonia by an amine as catalyst⁶⁹), and two silica aerogels (AERs). Additionally, for comparison were tested a hexagonal silica mesoporous molecular (MMS), to be exact, the MCM-41,^{70–72} which is ordered, but not crystalline, because of the lack of precise atomic positioning in the pores' wall structure;⁷³ one unidirectional 12-membered ring (MR) channels silica molecular sieve (MS), that is, SSZ-24, which is the siliceous counterpart of AlPO₄-5, showing the AFI framework;^{74–77} and two synthetic molecular sieves (MSs) with a high Si/Al relation, that is, two ZSM-5 and the extremely high Si/Al relation molecular sieve named dealuminated Y (DAY). The ZSM-5 is a 10MR molecular sieve showing the MFI framework type and the DAY is a 12MR molecular sieve exhibiting the FAU framework type.⁷⁷ These materials were studied with scanning electron microscopy (SEM), thermogravimetric analysis (TGA), small-angle X-ray scattering (SAXS), diffuse reflectance infrared Fourier transform spectrometry (DRIFTS), and adsorption of nitrogen at 77 K and carbon dioxide at 273 K.

Subsequently, the present paper has two major components. First, the SEM, TGA, and SAXS study of the silica xerogels and the DRIFTS study of the dehydrated silica surface will help us in the thorough characterization of the large group of structurally different studied materials. Second, the experimental and theoretical study of carbon dioxide adsorption in porous silica and the DRIFT study of carbon dioxide adsorbed on the surface of the different tested silicas were carried out to investigate the interaction of the carbon dioxide molecule and the silica surface.

2. Experimental Section

2.1. Materials and Synthetic Procedure.

All the consumed chemicals were analytical grade without additional purification. The water used in the synthesis process was bidistilled.

The sphere packing (SP) (Stöber silica) and particle packing (PP) silicas were synthesized with the help of the sol–gel processing method, specifically, the Stöber–Fink–Bohm (SFB) method^{65,68} and a modification of this method.⁶⁹ The batch composition for the synthesis of Stöber silica microspheres is

TABLE 1: Batch Composition for the Synthesis of the Silica Sphere Packing (SP) Materials

sample	TEOS ^b [ml]	DDW ^b [ml]	MeOH ^b [ml]	EtOH ^b [ml]	isoprop ^b [ml]	NH ₄ OH ^b [ml]
SP-80 ^a	1.5	0	30	0	0	6.0
SP-69B ^a	1.5	0.6	0	0	30	6.0
SP-FM3a ^a	2.2	0.6	0	30	0	3.6

^a SP means sphere packing silica xerogels. ^b TEOS is tetraethyl orthosilicate (TEOS), DDW is distilled water, MeOH is methanol, EtOH is ethanol, and isoprop is isopropanol. The ammonium hydroxide is 40 wt % NH₄OH in water.

TABLE 2: Batch Composition for the Synthesis of the Silica Particle Packing (PP) Materials

sample	TEOS ^b [ml]	DDW ^b [ml]	NH ₄ OH ^b [ml]	amine [ml]	MeOH ^b [ml]	EtOH ^b [ml]
PP-70bs2 ^a	0.25	0	0	2	0	10
PP-68bs1E ^a	0.25	0	0	1	10	0
PP-74bs5 ^a	0.35	2	0	2.5	9	1
PP-75bs1 ^a	0.35	0	0	2.5	10	0

^a PP means particle packing silica xerogels. ^b TEOS is tetraethyl orthosilicate (TEOS), DDW is distilled water, MeOH is methanol, and EtOH is ethanol. The ammonium hydroxide is 40 wt % NH₄OH in water.

presented in Table 1.^{65,68} To prepare the particle packing (PP) silica, some modifications to the SFB method were introduced, concretely, the change of ammonia by an amine as catalyst.⁶⁹ In Table 2 are reported the recipes used to synthesize the PP materials. The source materials for the synthesis were tetraethyl orthosilicate (TEOS), distilled water (DDW), methanol (MeOH), isopropanol, and ammonium hydroxide (40 wt % NH₄OH in water).

The two silica aerogel samples were synthesized applying a sol–gel procedure different from those previously described. The batch preparations were as follows:^{12,78}

(1) Ethanol (70 mL) + DDW (140 mL) + 30% aqueous ammonia solution (0.55 mL) + 0.5 M ammonium fluoride solution (2.4 mL) are mixed with agitation.

(2) TEOS (100 mL) + ethanol (80 mL) are also mixed.

(3) The solution number (1) is gradually added to solution number (2), and the mixture is intensively stirred at room temperature for 0.5 h.

(4) The products were aged at 300 K, during 14 days (AER-309) and 21 (AER-909) days. The obtained aged gels were supercritically dried to get two aerogel samples. The procedure applied to get the aerogels was the following:

(1) The samples were flushed three times with liquid CO₂ at 100 bar and 300 K during 3 h for each flush.

(2) Thereafter, the temperature was increased to 313 K and at the same pressure the samples were flushed with gaseous CO₂ at 100 bar during 6 h (AER-309) and 24 h (AER-909).

The supercritical drying process was carried out in the HELIX supercritical dryer developed and supplied by Applied Separations Inc., Allentown, PA.

The MMS-MCM-41, that is, the hexagonal phase of the family of mesoporous molecular sieves (MMSs), was used in the present study as a standard because it is a very well studied silica surface.^{79,80} This material is generally synthesized in basic solutions in which silicate oligoanions are structured by a cationic surfactant; postsynthetic removal of the surfactant yields the ordered mesoporous material.⁷¹ The MCM-41 used in the present study as a standard was synthesized^{68,69} using the common procedures reported in the literature.^{71,80}

The MS-SSZ-24 was provided by R. Lobos.^{74–76} The tested MS-DAY was the DAY-20F (Si/Al = 20) provided by Degussa AG, Germany,⁸¹ and the MS-ZSM-5, both 3020 and 5020, were provided by the PQ Corporation Malvern, PA.¹⁰

2.2. Characterization Methods. **2.2.1. Scanning Electron Microscopy.** The scanning electron microscopy (SEM) study was performed with a JEOL CF 35 scanning electron microscope in secondary electron mode at an accelerating voltage of 25 kV to image the surface of the studied samples. These samples were attached to the sample holder with an adhesive tape and then coated under vacuum by cathode sputtering with a 30–40 nm gold film prior to observation. The surface morphology was revealed from SEM images, and the average grain size was estimated, albeit qualitatively.

2.2.2. Nitrogen and Carbon Dioxide Adsorption. To measure the specific surface area, the pore volume and the pore size distribution (PSD) of the produced samples were obtained in a Quantachrome Autosorb-1 automatic physisorption analyzer, with the adsorption isotherms of N₂ at 77 K in samples previously degassed at 573 K during 7 h in high vacuum (10⁻⁶ Torr).^{9,10} With the help of the N₂ adsorption isotherms, the micropore volume, W^{Mic} was measured using the Dubinin^{58–65} and the *t*-plot^{7,9} methods and the specific surface area, S^{BET} , applying the Brunauer–Emmett–Teller (BET) method.^{3,7,9,53} For the calculation of the pore size distribution (PSD), the density functional theory (DFT) method was employed.⁹ From this data was calculated the DFT pore volume (W) and the DFT pore width mode (d^{Mes}). For the calculation of the pore size distribution (PSD) in the micropore region, the Saito–Foley (S-F) method was applied; from this data was calculated the SF pore width mode (d^{Mic}).¹⁰

Additionally, to study carbon dioxide adsorption, the adsorption isotherms of CO₂ at 273 K in samples degassed at 573 K during 3 h in high vacuum (10⁻⁶ Torr) were obtained, in an upgraded Quantachrome Autosorb-1 automatic physisorption analyzer. In this case, because the carbon dioxide vapor pressure, P_0 , at 273 K is high, that is, $P_0 = 26\ 141$ Torr,⁵² we will be working in the following relative pressure range: $0.00003 < P/P_0 < 0.03$. Experience indicates that the adsorption process in this range is very well described by the Dubinin adsorption isotherm equation in the case of carbonaceous materials⁵⁸ and other adsorbents.⁵⁹ The Dubinin–Astakhov (D-A) adsorption isotherm equation can be represented in a log–log scale as follows^{57–61}

$$\ln(n_a) = \ln(N_a) - \left(\frac{RT}{E}\right)^n \ln\left(\frac{P_0}{P}\right)^n \quad (1)$$

This equation describes the relation between the amount adsorbed, n_a , and the inverse of the relative pressure, that is, P_0/P , where E is a parameter named the characteristic energy of adsorption, N_a is the maximum amount adsorbed in the volume of the micropore, and n ($1 < n < 5$) is an empirical parameter. This equation is a very powerful tool for the description of the experimental data of adsorption in microporous material.^{9,10,57–64} The fitting process of eq 1 allows us to calculate the best fitting parameters, that is, N_a , E , and n . If n is considered a constant, for example, $n = 2$, we will get the Dubinin–Radushkevich (D-R) equation that will be the concrete equation applied here. With the help of the CO₂ adsorption isotherms and eq 1 with $n = 2$, the micropore volume, $W_{\text{MP}} = N_a V_L$ (where V_L is the molar volume of CO₂ at 273 K) and the characteristic energy of adsorption, E [kJ/mol], were then measured.^{58–64}

2.2.3. Thermogravimetric Analysis. The TGA testing process was carried out with a TA Q-500 equipment.¹⁰ To perform the TGA test, the samples were placed into a ceramic sample holder, which was suspended from an analytical balance. The sample holder was then heated according to a predetermined thermal cycle, that is, the temperature was linearly scanned, from 23 to 800 °C at a heating rate of 5 °C/min in a flow of 100 mL/min of the purge gas, which is pure N₂. The data collection, the temperature control, the programmed heating rate, and the gas flow control were automatically controlled by the software of the TA TQ500 TGA. The TGA data were collected as a wt % versus T (°C) profile, where $\text{wt \%} = (M_t/M_0) \times 100$ is the percent ratio of the sample mass during the thermal treatment, M_t , and the initial mass of the sample, M_0 .

2.2.4. Small-Angle X-ray Scattering. The small-angle X-ray scattering (SAXS)^{82–92} experiment was carried out with a Bruker D8 Advance system in transmission configuration. The SAXS data are normally plotted as $I(q)$ (intensity) versus $q = (4\pi/\lambda)\sin(\theta)$ ($\lambda = 0.1542$ nm) on a log–log scale. In these plots are normally observed the Porod power law region⁸⁸

$$\ln[I(q)] = \ln B - 4 \ln[q] \quad (2)$$

in which B is a constant and the Guinier power law region⁸⁷

$$I(q) = G \exp\left[-\frac{R_g}{3}q^2\right] \quad (3)$$

where G is a constant and R_g is the radius of gyration. We will only apply here the SAXS data to calculate the primary particle diameter, ϕ_{VIS} , using the Porod data, as follows⁸⁸

$$\phi_{\text{VIS}} = \frac{6Q}{\pi B} \quad (4)$$

where

$$Q = \int_0^\infty q^2 I(q) dq \quad (5)$$

is the Porod invariant.

2.2.5. Diffuse Reflectance Infrared Fourier Transform Spectrometry. To get the diffuse reflectance infrared Fourier transform spectra, a Thermo Scientific Nicolet iS10 FTIR spectrometer with the Smart Collector for diffuse reflectance analysis and the environmental chamber for the Smart Collector were used. The spectra were collected with a resolution of 4 cm⁻¹, and 100 scans per sample were made.

To get the sample spectrum in the case of the dehydrated samples, a background with KBr (FTIR pure, provided by Nicolet) located in the sample holder of the environmental chamber was made applying the same conditions used to get, later, the sample spectra. To dehydrate the samples, they were heated at 300 °C under a N₂ (Praxair, 99.99%) flow at a rate of 50 cc/min during 2 h. Lastly, the spectra of the dehydrated silica were obtained with the sample inside the environmental chamber, at room temperature, under a N₂ (Praxair, 99.99%) flow at a rate of 50 cc/min.

To get the IR spectra of carbon dioxide adsorbed on the silica surfaces, the background taken was the sample dehydrated at 300 °C. Thereafter was passed a flow of CO₂ (Praxair, 99.99%)

TABLE 3: Morphological Data of the Silica Sphere Packing Materials and the MMS-MCM-41^a

sample	S^{BET} [m ² g ⁻¹]	W^{Mic} [cm ³ g ⁻¹]	W^{DFT} [cm ³ g ⁻¹]	d^{Mic} [nm]	d^{Mes} [nm]	ϕ^{SEM} [nm]
SP-80 ^b	400 ± 100	0.16	0.49 ± 0.15	0.57	3.9	200–300
SP-69b ^b	300 ± 100	0.06	0.52 ± 0.15	0.59	8.1	300–400
SP-FM3a ^b						200–300
MCM-41	800 ± 100		1.69 ± 0.15		3.5	

^a The adsorption data were taken from ref 68. ^b SP means sphere packing silica xerogels.

TABLE 4: Morphological Data of the Particle Packing Materials and Both Aerogels^a

sample	S^{BET} [m ² g ⁻¹]	W^{Mic} [cm ³ g ⁻¹]	W^{DFT} [cm ³ g ⁻¹]	d^{Mic} [nm]	d^{Mes} [nm]
PP-70bs2 ^b	1600 ± 500	0.18 ± 0.05	3.0 ± 0.5	0.55	6.5
PP-74bs5 ^b	1200 ± 400	0.14 ± 0.05	1.7 ± 0.5	0.57	6.1
PP-68bs1e ^b	1500 ± 500	0.27 ± 0.05	2.4 ± 0.5	0.55	8.1
PP-75bs1 ^b	1400 ± 500	0.16 ± 0.05	2.7 ± 0.5	0.57	12.5
AER-309 ^b	500 ± 100	0.16 ± 0.05	4.2 ± 1.0	0.58	50.0
AER-909 ^b	1000 ± 200	0.4 ± 0.1	2.0 ± 1.0	0.57	7.3

^a The adsorption data of the particle packing (PP) silica were taken from ref 69. ^b PP means particle packing silica xerogels, and AER are silica aerogels.

at a rate of 50 cc/min during 3 min. The samples were then purged under a N₂ (Praxair, 99.99%) flow at a rate of approximately 50 cc/min during 1 min and, for some samples, for 7 min to desorbs the weakly bonded carbon dioxide. Finally, the spectra were obtained with the sample inside the environmental chamber to get the spectra of the carbon dioxide molecule adsorbed on the silica surface.

3. Results and Discussion

3.1. Silica Characterization. 3.1.1. Silica Morphology. All the silica sphere packing (SP) and particle packing (PP) materials, excluding the SP-FM3a-GeO, were previously morphologically characterized with the help of nitrogen adsorption and SEM.^{68,69} These data are reported in Tables 3⁶⁸ and 4.⁶⁹ It is evident from these results that the SP and PP samples show a complex pore structure with a considerable micropore region and a very developed mesopore region, as is revealed by the large total pore volume (W^{DFT}) reported.^{68,69}

The aerogels' morphological characterization was also determined with the help of nitrogen adsorption at 77 K in order to measure the S^{BET} , W^{Mic} , W , d^{Mic} , and d^{Mes} . The results obtained are reported in Table 4. It is evident from the reported data that both aerogel samples show also a complex pore structure with a considerable micropore region and a very developed mesopore region. Below will be given more details about the morphology of all these silicas.

The MS-SSZ-24 was characterized by the group who synthesized this sample.^{74–76} The MS-DAY⁸¹ and both MS-ZSM-5¹⁰ were previously structurally and morphologically characterized.¹⁰ The micropore volume of these samples, measured with the help of nitrogen adsorption, are shown in Table 5.^{64,81}

In Figure 1 are reported the SEM images of the sphere packing silicas SP-80 and SP-FM3a-GEO. In these microographies are evidently shown the spherical form of the Stöeber silica. The diameters of these spheres, ϕ^{SEM} [nm], are reported in Table 3. Also, in Figure 1 is shown a micrograph of the particle packing silica PP-68bs1e. In this micrography is obviously revealed that the spherical geometry was broken

TABLE 5: Morphological Data of the MS-DAY, MS-ZSM-5 (3020), and MS-ZSM-5 (5020)^{10,81,103}

sample	W^{Mic} [cm ³ g ⁻¹]	Saito–Foley pore diameter [nm]
MS-DAY ^a	0.30 ± 0.01	0.60
MS-ZSM-5(3020) ^a	0.11 ± 0.01	0.54
MS-ZSM-5(5020) ^a	0.12 ± 0.01	0.54

^a MS means molecular sieves.

because of the use of an amine instead of ammonium hydroxide as a catalyst.⁶⁹ The diameter of the particles PP-68bs1e is $\phi = 1\text{--}5 \mu\text{m}$.

The pore size distribution (PSD), in the micropore range, calculated with the help of the Saito–Foley method, specifically for SP-69b, PP-68bs1e, MS-ZSM-5-5020, and MS-DAY, which are typical SP, PP, and MS, are shown in Figure 2. In Tables 3 and 4 are reported the SF-PSD pore width mode d^{Mic} [nm].

Small-angle X-ray scattering^{82–92} (SAXS) is one of the main tools applied to investigate the morphology of particle aggregates because it allows probing a structure over several orders in length scale in the nanoregion, including both primary particles and aggregates.^{83–88} In Figure 3 are shown the SAXS data corresponding to the PP-68bs1e. The results obtained for these parameters are reported in Table 6. It is now necessary to state that we did not study here the SP samples by SAXS because they are very well studied with this method.^{88–92}

The previously reported morphologic data of the SP and PP silica samples indicate that these adsorbents have a complex pore structure, including micropores and mesopores. This morphology is a result of the particular internal morphology of the SP and PP silicas, which are composed of the secondary particles, evidenced by SEM where these agglomerates are composed of primary particles. That is, the observed morphology is explained by the agglomeration of the primary particles, revealed with the help of the SAXS study, to form the secondary particles because in the agglomeration process are created void spaces between the primary particles. This morphology will be reflected in the adsorption of carbon dioxide as will be later explained.

The TGA reported here was taken under a N₂ flow from 25 to 800 °C. The thermal gravimetric profiles of the SP silicas are shown in Figure 4; those of the PP silicas in Figure 5 and the TG of the standards MMS, the MS silica, and a high silica MS are shown in Figure 6.

At relatively low temperatures, that is, below 200 °C, takes place the release of loosely linked water. The differential TGA peaks of dehydration and dehydroxylation were applied to determine the position of this point. It was set at 200 °C (see Figure 7); at temperatures higher than 200 °C, the surface silanol groups begin their condensation to form water molecules.⁹³ Finally, at 700–800 °C, only isolated silanols are present in the surface.⁹⁴

We have previously measured the specific surface area of the produced amorphous silica with the help of the BET method.^{68,69} This method shows normally a 20% relative dispersion of the results.³ However, for samples with a very high specific surface area, the relative error is bigger,^{9,10,68,69} that is, about 30%. In this regard, we will apply here an innovative methodology to confirm the BET data, applying the TGA profiles of the amorphous silica xerogels.

To calculate the silica specific surface area with the TGA data, a very well known fact⁹³ will be used, explicitly, that, in a fully hydroxylated silica, the specific amount of OH, that is, $\sigma \approx 4.5 \text{ OH/nm}^2$, can be considered a constant (the Kisieliov–

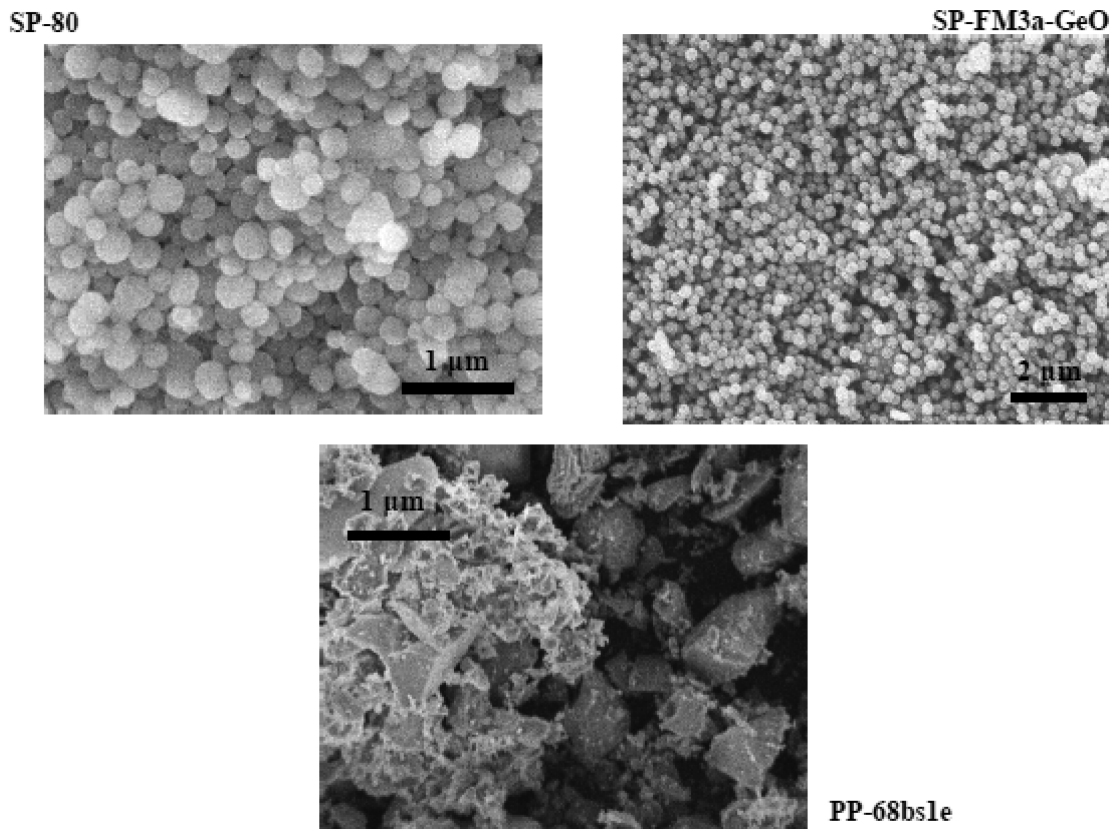


Figure 1. SEM micrographs of SP-80, SP-FM3a-GeO, and PP-68bs1e.

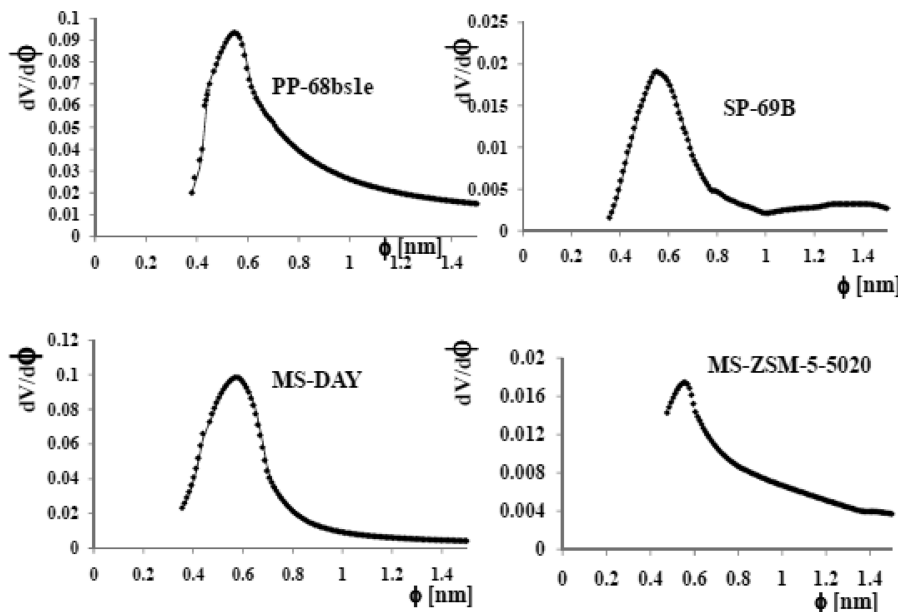


Figure 2. Saito–Foley pore size distribution (SF-PSD) of SP-69b, PP-68bs1e, MS-ZSM-5-5020, and MS-DAY.

Zhuralev constant), independent of the silica type.^{12,95–97} In this regard, the specific amount of OH can be calculated with the help of the TGA profile, as follows⁹³

$$\sigma = 2 \left(\frac{\Delta W_{\text{H}_2\text{O}}}{M_{\text{H}_2\text{O}} N_A S} \right) \quad (6)$$

where $\Delta W_{\text{H}_2\text{O}} = \text{wt \% (200 }^{\circ}\text{C)} - \text{wt \% (700 }^{\circ}\text{C)}$, in which $\text{wt \%} = (M_T/M_0) \times 100$ is the percent ratio of the sample mass

during the thermal treatment, M_T is the mass of the sample at temperature T , and M_0 is the initial mass of the sample. The factor 2 implies that each water molecule requires two OH groups to be formed; $M_{\text{H}_2\text{O}}$ is the molecular weight of water, N_A is the Avogadro number, and S is the specific surface area of the silica.

The use of the TGA method for this purpose has a weak point: the determination of the end of the process of physically adsorbed water release, that is, the separation of the dehydration and dehydroxylation processes.⁹⁴ In the present study, as was

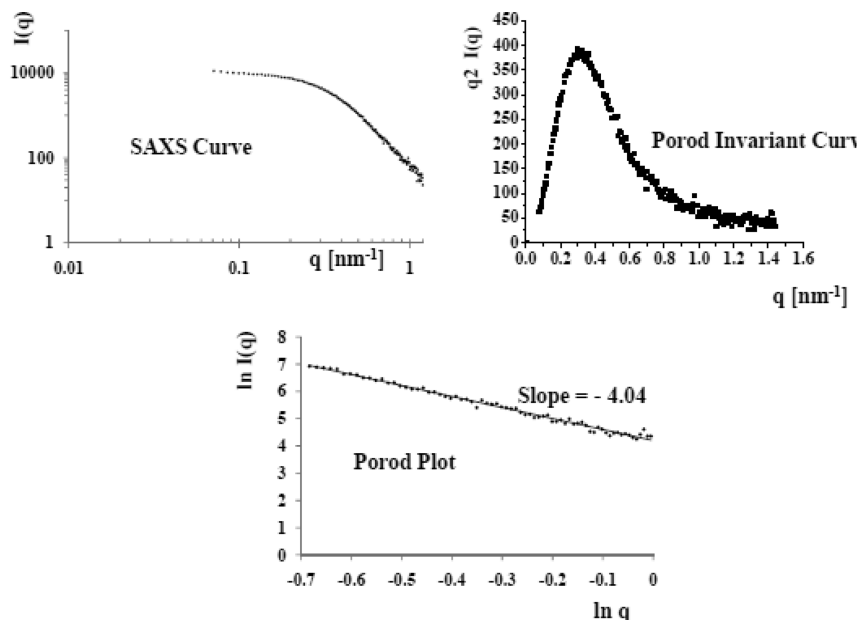


Figure 3. SAXS data corresponding to the PP-68bs1e.

TABLE 6: SAXS Parameters of PP 68bs1e

sample	B [nm^{-4}]	Q [nm^{-3}]	ϕ_{VIS} [nm]	$R^2/3$ [nm^2]	ϕ_s [nm]
PP-68bs1e ^a	66.7	267.1	7.6	10.6	11.2

^a PP means particle packing silica xerogels.

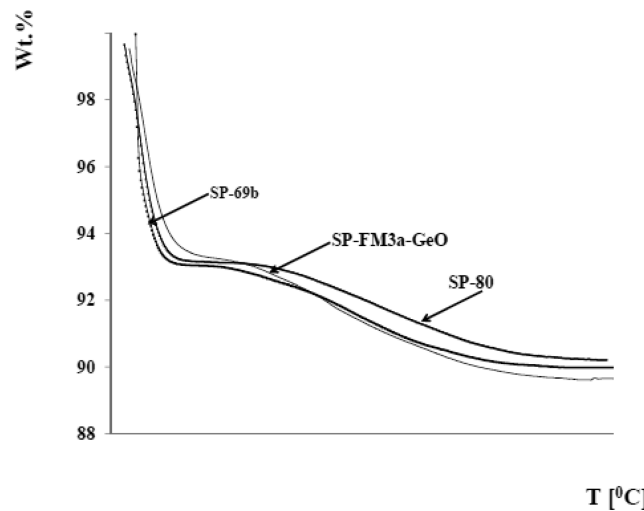


Figure 4. TG profiles of SP-80, SP-69b, and FM3a-GeO.

previously commented, we applied the differential TGA peaks of dehydration and dehydroxylation (see Figure 7) in order to determine this point.⁹⁸ If we then consider $\sigma = 4.5 \text{ OH}/\text{nm}^2$ a constant, then, with the expression

$$S^{\text{TG}} = 2 \left(\frac{\Delta W_{\text{H}_2\text{O}}}{M_{\text{H}_2\text{O}} N_A \sigma} \right) \quad (7)$$

we can calculate the specific surface area, with the help of the TGA method. In Table 7 are reported the obtained values. These results coincide within the error magnitude with the S^{BET} values reported in Tables 3⁶⁸ and 4.⁶⁹ However, these results do not exhibit a big dispersion, as was the case for the values reported in Table 4; that is, the relative error was 15–20%. With a novel

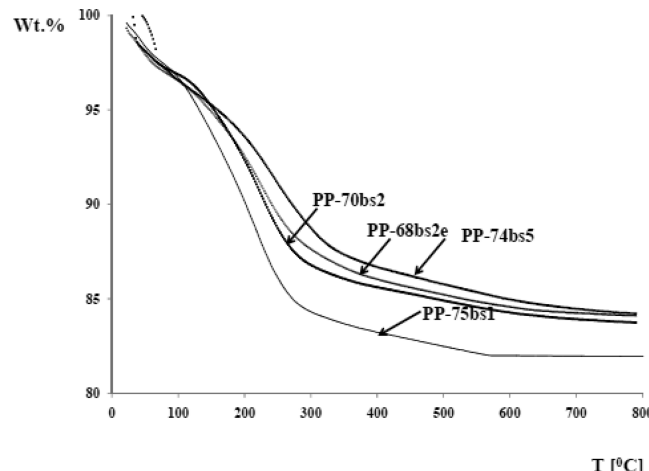


Figure 5. TG profiles of PP-70bs2, PP-74bs5, PP-68bs1e, and PP-75bs1.

methodology specifically developed for the calculation of the specific surface area of silica, the extremely high specific surface area of the PP silica was confirmed and more precise and accurate values were obtained.

The specific surface area data reported indicate that the PP and AER samples exhibit a high specific surface area. This fact points to the potential application of these materials in the adsorption of polar molecules.^{7,9,10}

With the help of the figures reported for the specific surface area, it is possible to calculate a diameter of the primary particles, that is, ϕ^{TG} , applying the following expression¹⁰

$$\phi^{\text{TG}} = \frac{6}{S\rho} \quad (8)$$

where $\rho = 2.2 \text{ g/cm}^3$ is the density of silica. The calculated values are reported in Table 7. It is evident that the reported values for the particle diameter calculated with the specific surface area are lower than those calculated by SAXS. Other authors have also found that the silica primary particle diameters measured with the SAXS methodology are, in some cases, larger

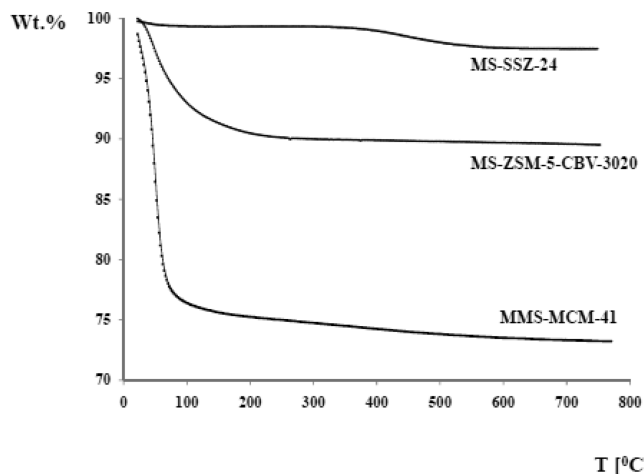


Figure 6. TG profiles of MS-SSZ-24, MS-ZSM-5-3020, and MMS-MCM-41.

than the diameter measured with the help of eq 8, applying the BET specific surface area.⁹³

The results reported above allow us to state that the studied amorphous sphere packing and particle packing silicas have a particular internal morphology that is composed of the secondary particles, evidenced by SEM (see Figure 1), that is, aggregates whose diameters are around 300 nm for the SP and 1000 nm for the PP (see Figure 1 and Tables 3 and 4). These agglomerates are composed of primary particles of around 15–20 nm^{88–91} for the SP silica and 7 nm for the PP silica (see Table 6). The observed microporosity (Figure 2 and Tables 3 and 4) is explained by the agglomeration of the primary particles to form the secondary particles because in the agglomeration process are created void spaces between the primary particles. To be exact, the SP, PP, and AER samples show micropores with $d^{\text{Mic}} = 0.56\text{--}0.59$ nm (see Figure 2 and Tables 3 and 4) and mesopores with $d^{\text{Mes}} = 4\text{--}8$ nm for the SP, $d^{\text{Mes}} = 6\text{--}12$ nm

TABLE 7: Specific Surface Area Calculation Applying the TGA Data

sample	$S^{\text{TGA}} [\text{m}^2 \text{ g}^{-1}]$	$n^{\text{OH}} [\text{OH m}^{-2}]$	$\phi^{\text{S}} [\text{nm}]$
SP-69b ^a	500 ± 100	4.5 ± 0.5	5 ± 1.0
SP-80 ^a	500 ± 100	4.5 ± 0.5	5 ± 1.0
SP-FM3a-GeO ^a	500 ± 100	4.5 ± 0.5	5 ± 1.0
PP-70bs2 ^a	1300 ± 200	4.5 ± 0.5	2 ± 0.5
PP-74bs5 ^a	1300 ± 200	4.5 ± 0.5	2 ± 0.5
PP-68bs1e ^a	1300 ± 200	4.5 ± 0.5	2 ± 0.5
PP-75bs1 ^a	1200 ± 200	4.5 ± 0.5	2 ± 0.5

^a SP means sphere packing silica xerogels, and PP means particle packing silica xerogels.

for the PP, and bigger for the aerogels, that is, $d^{\text{Mes}} = 7\text{--}50$ nm. The specific surface areas of the PP and one of the AER silicas are 2–3 times bigger than those of the SP silicas and also 1.5 bigger than those of the MMS-MCM-41. These facts make the PP silica and one of the AER-909 samples very good materials for large specific surface area applications as adsorbents and catalyst supports.

Now, it is necessary to emphasize the fact that the micropore diameter measured for the tested silica is very similar to the pore size of the 10 MR channel of the MFI framework, corresponding to the molecular sieves ZSM-5 and silicalite.⁷⁷

Additionally, the obtained data indicate that the morphologies of the MMS-MCM-41, the MS-DAY, MS-ZSM-5, and MS-SSZ-24 are typical of these materials, as reported in the literature.^{10,70–77} It is necessary now to state that the synthesized amorphous silica includes a micropore region comparable or bigger than that of all-silica zeolite. This micropore volume has similar adsorption properties than those of crystalline silica, and additionally, silica exhibits a highly developed mesopore region where adsorption takes place also. Consequently, for those applications where the specific surface area is important, the obtained amorphous silicas are better adsorbents. On the other hand, the mesoporous molecular sieves (MMSs) are better for

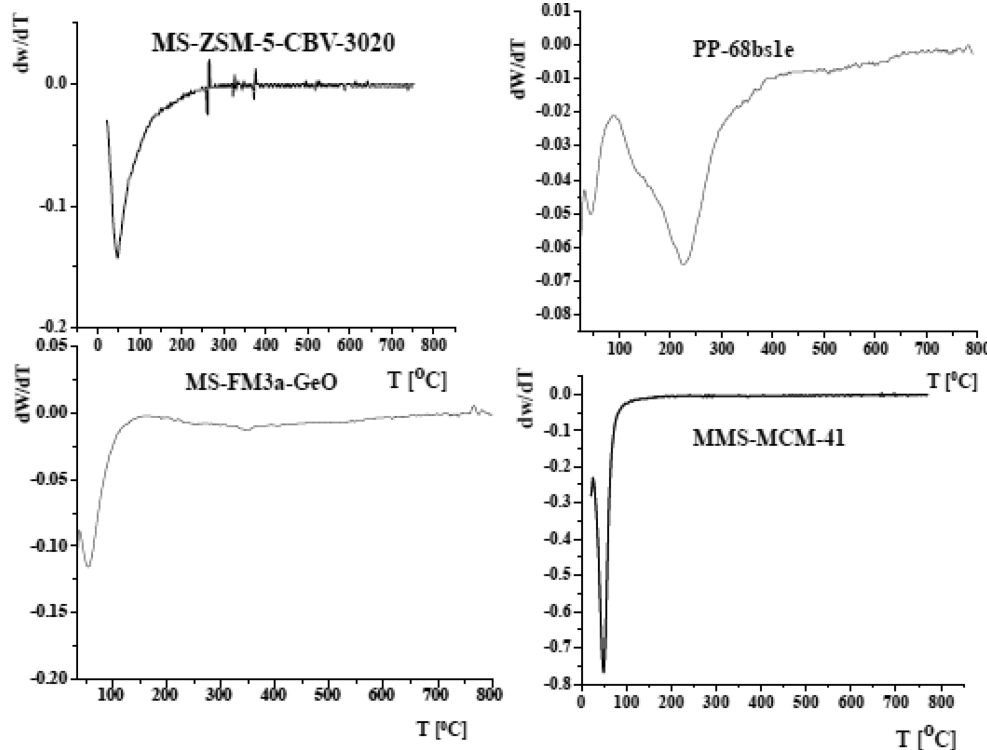


Figure 7. Derivative of the TG profiles of MS-ZSM-5-3020, MMS-MCM-41, SP-FM3a-GeO, and PP-68bs1e.

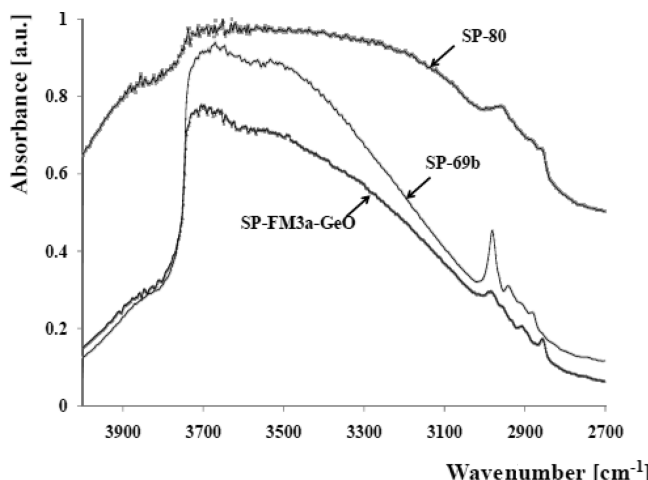


Figure 8. DRIFTS spectra of the dehydrated sphere packing silica at 300 °C: SP-80, SP-69B, and FM3a-GeO.

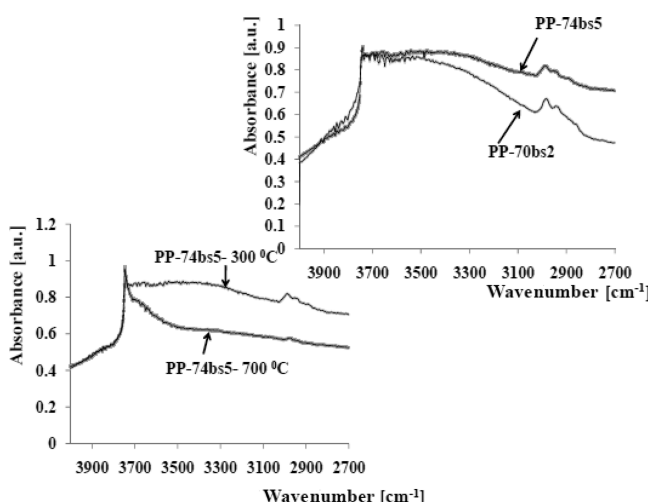


Figure 9. DRIFTS spectra of the dehydrated particle packing silicas, PP-70bs2 and PP-74bs5, at 300 °C and the PP-74bs5 heated at 700 °C.

applications where order is important; however, the MMSs do not show a micropore adsorption volume, which is very important for many applications of silica as adsorbents.

3.1.2. Silica Surface Chemistry. To complete the characterization of the tested silica, we need to study its surface chemistry. For the study of this topic, the silica samples were carefully dehydrated in the environmental chamber for the Smart Collector of the Nicolet iS10 FTIR spectrometer, as was previously explained. In Figure 8 are shown the DRIFT spectra of the dehydrated sphere packing silica in the range between 4000 and 2700 cm^{-1} . In Figure 9 are shown the DRIFT spectra of the dehydrated particle packing silica in the range between 4000 and 2700 cm^{-1} , and finally, in Figure 10 are shown the DRIFT spectra of the dehydrated AER-309 and the MMS-MCM-41, the MS-SSZ-24, and the MS-ZSM-5-5020, also in the range between 4000 and 2700 cm^{-1} .

In relation to the bands present in the recorded DRIFTS spectra, the most important are those related to the hydroxyl functionalities, that is, vicinal, geminal, and isolated silanol sites,^{99,100} explicitly, the O–H fundamental stretching vibration range, that is, 3800–3000 cm^{-1} . The terminal free OH group, which is not H-bonded, shows a narrow absorption band at about 3720–3730 cm^{-1} , whereas the vicinal and germinal OH groups, which are H-bonded, show a broad absorption band, which

results from the superposition of different hydrogen-bonded interacting OH groups.¹⁰¹ These bands are present in all the obtained spectra (see Figures 8–10). Specifically, the pattern of bands shown by these spectra is, in a general sense, similar for all the studied samples. Consequently, the studied samples have a surface chemistry typical of silica, showing free silanol groups and vicinal and geminal silanol groups. Additionally, in the DRIFTS spectrum of the sample PP-74bs5 (Figure 9) after heating it at 700 °C, an increase in the intensity of the free OH group and a decrease of the band corresponding to vicinal and germinal OH groups are evident. This fact corresponds to the effect of heating a silica, whose outcome is the production of a siloxane site, one water molecule, and an isolated SiOH group.⁹⁴

In a closer look, it is evident that the surface chemistries of both the SP and the PP silicas are very similar, exhibiting a big amount of vicinal hydroxyl groups, which made it hydrophilic; that is, these samples show a water release process during heating. On the other hand, the AER-309, the MMS, and the MS silica samples show a somewhat different distribution of the OH groups. The studied amorphous sphere packing (SP) and particle packing silicas exhibit free silanol groups and vicinal and geminal silanol groups within their microporosity and mesoporosity (Figures 8 and 9), that is, a typical silica surface chemistry. However, for the MMS and both MS samples, the silanol group is stronger than for the SP, PP, and AER samples; that is, an intense band at about 3730 cm^{-1} , corresponding to the silanol groups,¹⁰² is observed (see Figures 8–10). This fact explains why these samples are hydrophobic.⁷ That is, these samples do not show a water release process during heating. On the contrary, it shows only a fast dehydroxylation. Additionally, it is obvious that, in the MS samples, bridged OH groups are present (see Figure 10); that is, the DRIFTS spectra of the MS show a band around 3650 cm^{-1} related to the bridging hydroxyl groups.¹⁰² The AER sample exhibits two peaks, one at around 3630 cm^{-1} and the other at around 3560 cm^{-1} , related to vicinal OH groups, but with a different distribution than those exhibited for the SP and PP silicas. Independent of the general similitude, some differences are found between the tested silica samples.

The obtained results indicate that the impregnation of amines or the loading of alkali metals and other metals³³ is possible in the SP, PP, and AER samples because of their high specific surface area covered by hydroxyl groups, which are, indeed, particularly reactive.^{7,9,10,12}

3.2. Interaction of Carbon Dioxide with the Surface of the Studied Silica. **3.2.1. Measurement of the Micropore Volume with Carbon Dioxide Adsorption.** In Figure 11 are reported the Dubinin plots of the adsorption isotherms of carbon dioxide at 273 K on the silicas SP-80, SP-69B, FM3a-GeO, PP-68bs1e, and PP-75bs1 and, in Figure 12, the Dubinin plots of the adsorption isotherms of carbon dioxide at 273 K on MMS-MCM-41, MS-ZSM-5-5020, and MS-DAY.

The values of the micropore volume measured with the help of carbon dioxide adsorption, $W_{\text{MP}}^{\text{CO}_2}$, are reported in Table 8. This parameter was measured by fitting eq 1, with $n = 2$, to the data reported in Figures 11 and 12. The reported results indicate, as was previously shown with the help of nitrogen adsorption at 77 K, that the samples exhibit a developed micropore region, in addition to the mesopore portion of the silica framework. It is necessary to state now that carbon dioxide adsorption takes place only in the micropore region. This is evident because of the excellent fitting of the obtained data by the D-R isotherm (see Figures 11 and 12).

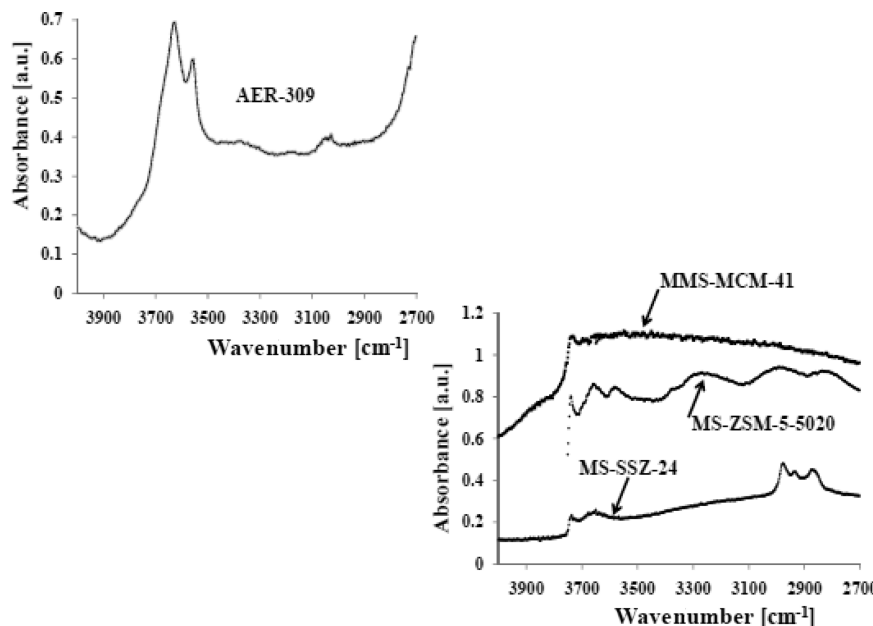


Figure 10. DRIFTS spectra at 300 °C of the dehydrated AER-309, MMS-MCM-41, MS-ZSM-5-5020, and MS-SSZ-24.

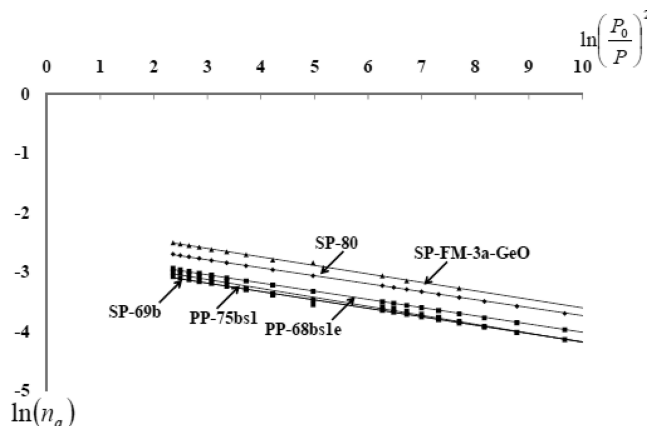


Figure 11. Dubinin plots of the adsorption isotherms of carbon dioxide at 273 K on SP-80, SP-69B, FM3a-GeO, PP-68bs1e, and PP-75bs1.

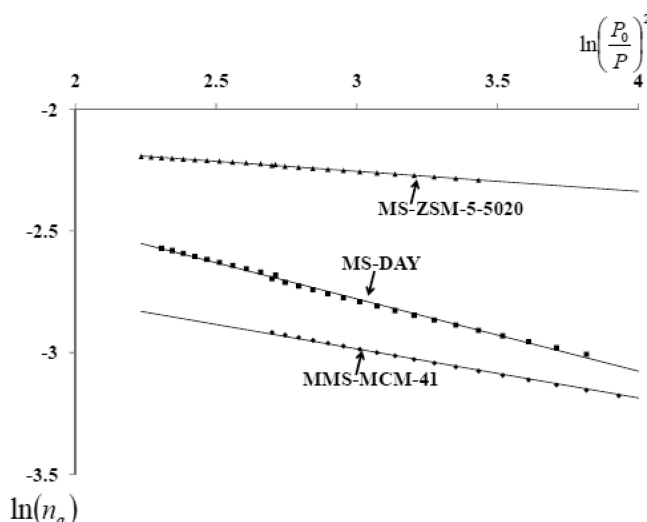


Figure 12. Dubinin plots of the adsorption isotherms of carbon dioxide at 273 K on MMS-MCM-41, MS-ZSM-5-5020, and MS-DAY.

The developed micropore adsorption space measured with carbon dioxide adsorption is in agreement with the nitrogen adsorption morphological data discussed in the previous section.

TABLE 8: Parameters Calculated with the Dubinin–Radushkevish Equation

sample	R^2	E^{CO_2} [kJ/mol]	$q_{iso}^{CO_2}(0.37)$ [kJ/mol]	$W_{MP}^{CO_2}$ [cm ³ /g]
SP-69 ^a	0.9997	24	28	0.21
SP-80 ^a	0.9999	24	28	0.13
SP-FM3a-GeO ^a	0.9998	24	28	0.23
PP-68bs1e ^a	0.9998	24	28	0.17
PP-75bs1 ^a	0.9998	23	27	0.23
MMS-MCM-41 ^a	0.9990	19	22	0.24
MS-ZSM-5-5020 ^a	0.999	33	38	0.17
MS-DAY ^a	0.9985	17	20	0.33

^a SP means sphere packing silica xerogels, PP means particle packing silica xerogels, MS are molecular sieves, and MMS is a mesoporous molecular sieve.

3.2.2. Heat of Adsorption. We know that, in general, if a molecule contacts the surface of a solid adsorbent, it becomes subjected to diverse interaction fields, such as the dispersion energy, ϕ_D , repulsion energy, ϕ_R , polarization energy, ϕ_P , field dipole energy, $\phi_{E\mu}$, field gradient quadrupole energy, ϕ_{EQ} , and some specific interactions, such as the acid–base interaction, ϕ_{AB} .^{102,103} Normally, it is also necessary to take into account the adsorbate–adsorbate interaction energy, ϕ_{AA} .

Dispersion and repulsion are the fundamental forces present during physical adsorption in all adsorbents. In the case of molecules, such as H₂, Ar, CH₄, N₂, and O₂, these are the only forces present; given that the dipole moments of these molecules is zero, the quadrupole moment is very low or absent, and the polarization effect will be only noticeable in the case of adsorbents with high electric fields.^{2,4,6,9,10,64} Dispersion and repulsion interactions are present in all adsorption gas–solid systems; therefore, they are nonspecific interactions.¹⁰⁴

The electrostatic interactions between the adsorbed molecule and the adsorbent framework, that is, ϕ_P , $\phi_{E\mu}$, and ϕ_{EQ} , depend on the structure and composition of the adsorbed molecule and the adsorbent itself. That is, the interaction between the adsorbent and molecules with, for example, a noticeable quadrupolar moment, such as the carbon dioxide molecule ($Q_{CO_2} = -4.3 \times 10^{-42}$ Cm²),¹⁰⁵ gives rise to specific interactions, where the combination of the dispersive and electrostatic

attractive interactions is normally stronger than merely the dispersion interactions. In the case of interest here, it is accepted that carbon dioxide interacts with surfaces through its dispersive and quadrupole moment interactions.^{7,9,10,104,106–108}

The parameters calculated with the D-R adsorption isotherm equation allow us to evaluate not only the micropore volume of the sample but also the adsorption interaction between the adsorbate and the adsorbent. To evaluate this interaction, the characteristic energy of adsorption, E , calculated by fitting eq 1, with $n = 2$, to the data reported in Figures 11 and 12 (see Table 8), will be used. The quantitative evaluation of the interaction between carbon dioxide and silica will be carried out with help of the isosteric heat of adsorption, q_{iso} .^{2,6,9,10} In this regard, we will show now that it is possible to calculate q_{iso} in an original way using only one isotherm as follows⁶¹

$$q_{\text{iso}}(\theta) = -\Delta G(\theta) + EF(T, \theta) \quad (9)$$

in which

$$\Delta G(\theta) = RT \ln\left(\frac{P}{P_0}\right) \quad \text{and} \quad F(T, \theta) = \frac{\alpha T}{2} \left(\ln\left[\frac{1}{\theta}\right]\right)^{\frac{1}{n}-1} \quad (10)$$

where $\theta = n_a/N_a$, $\alpha = -d \ln N_a/dT$, and E and n are the parameters of the Dubinin adsorption equation (in our case, $n = 2$, and E is reported in Table 8). It is also possible to assert that⁶¹ $E = \Delta G(1/e)$, where $\theta = 1/e$, in which $e \approx 2.71828183$ is the base of the Napierian logarithm system. Now, with the help of eqs 9 and 10, for $\theta = 1/e \approx 0.37$, it is possible to get the following equation:

$$q_{\text{iso}}(0.37) = -\Delta G(0.37) + EF(T, 0.37) = E[F(T, 0.37) - 1] \quad (11)$$

To calculate $F(T, 0.37)$ with the help of eq 11, we need trustworthy experimental calorimetric data reported in the literature. In this regard, the experimental heat of adsorption data that will be applied to compute $F(T, 0.37)$ is $q_{\text{iso}} = 22 \text{ kJ/mol}$ for the adsorption of carbon dioxide at 298 K, in the range of $0.1 < n_a < 0.7 \text{ mmol/g}$ in MCM-41.¹⁰⁹ Consequently, it is possible to estimate that $F(T, 0.37) \approx 2.16$. With the relation

$$q_{\text{iso}}(0.37) = 1.16E$$

were calculated the isosteric heats of adsorption (see Table 8).

The results reported in Table 8 indicate that the tested SP and PP silicas show similar values for the isosteric heat of adsorption. This value is also identical to the experimental isosteric heat of adsorption, $q_{\text{iso}} = 28 \text{ kJ/mol}$, measured for the adsorption of carbon dioxide at 296–306 K, in the range of $0.1 < n_a < 1.5 \text{ mmol/g}$, in silicalite.¹⁰⁸ The similarity between the values reported for the isosteric heat of adsorption of carbon dioxide on the tested SP and PP silicas and those reported for silicalite is due to the similitude between the silicalite porosity and surface chemistry and those of the tested silica in the micropore range. That is, the studied silica samples, in the micropore region, exhibit pore sizes in the range of $0.56 \text{ nm} < d^{\text{Mic}} < 0.59 \text{ nm}$, and the 10 MR channels of the MFI framework⁷⁷ of silicalite display pore openings of $0.51 \times 0.55 \text{ nm}^2$ and $0.53 \times 0.56 \text{ nm}^2$. Consequently, because, for porous materials with

TABLE 9: Physical Properties of Carbon Dioxide and the Oxide Ion^{103,116}

atomic species	polarizability $\alpha [10^{-24} \text{ cm}^3]$	magnetic susceptibility $\chi [10^{-29} \text{ cm}^3]$	diameter $d [\text{nm}]$	surface density $N_s [10^{18} \text{ at/m}^2]$
CO ₂	2.48	3.49	0.33	5.0
oxideion	2.50	1.30	0.28	13.1

a similar surface chemistry, the pore size is the main parameter in the determination of the adsorption heat in porous materials,^{103,110–112} then our conclusion reasonably results.

The previously described adsorption data indicate that the interaction of the carbon dioxide molecule with silica is not strong; that is, we are in the presence of a physical adsorption process, as is normally accepted for the adsorption of carbon dioxide on silica.¹¹³ It is accepted that this physical adsorption process binds the carbon dioxide molecule inside the silica surface micropores, by the influence of the dispersive forces and the attraction of the quadrupole interaction.^{106–108}

The strength of the dispersive potential, for the cylindrical pore geometry, for a relatively low coverage, can be calculated¹⁰³ following the methodology developed by Horvath–Kawazoe¹¹⁴ and Saito–Foley.¹¹⁵ With the help of this methodology, it is possible to show that $\xi_{\text{cal}}^{\text{CO}_2}(r_p)$, the enthalpy of adsorption for the cylindrical pore geometry, is given by¹⁰³

$$\xi_{\text{Dis-Int.}}^{\text{CO}_2}(r_p) = \frac{3}{4} \pi N_A \left(\frac{N_{\text{AS}} A_{\text{AS}}}{d^4} \right) \left(\sum_{k=0}^{\infty} \left[\frac{1}{2k+1} \left(1 - \frac{d}{r_p} \right)^{2k} \times \left\{ \frac{21}{32} \alpha_k \left(\frac{d}{r_p} \right)^{10} - \beta_k \left(\frac{d}{r_p} \right)^4 \right\} \right] \right) \quad (12)$$

where

$$A_{\text{AS}} = \frac{6mc^2\alpha_S\alpha_A}{\left(\frac{\alpha_S}{\chi_S} + \frac{\alpha_A}{\chi_A} \right)} \quad (13)$$

is one of the Kirkwood–Muller formula equations, in which m is the mass of an electron, c is the speed of light, α_A and α_S are the polarizabilities of the adsorbate and the adsorbent molecules, χ_A and χ_S are the magnetic susceptibilities of the adsorbate and the adsorbent, and r_p is the radius of the cylindrical pore. $d = d_S/2 + d_A/2$, where d_S is the diameter of the adsorbent (the oxide ion for silica) and d_A is the diameter of the adsorbate (carbon dioxide), N_{AS} is the number of solid molecules/surface units, and N_A is the Avogadro number. $\xi_{\text{Dis-Int.}}^{\text{CO}_2}(r_p)$ is given in J/mol if we apply SI units.

In Table 9^{103,116} are shown a set of values for the parameters, α , χ , d , and N_s , for CO₂ as an adsorbate and the oxide ion as an adsorbent. Subsequently, if we consider that the silica pores can be considered cylindrical, it is then possible to make a calculation of the contribution of the dispersive interactions, by the substitution of the physical properties of carbon dioxide and the oxide ion, reported in Table 9 and in eqs 12 and 13, and the values of the fundamental constants involved in the calculation, to get

$$\xi_{\text{Dis-Int.}}^{\text{CO}_2}(r_p) = 24.76 \times 10^3 \left(\sum_{k=0}^{\infty} \left[\frac{1}{2k+1} \left(1 - \frac{d}{r_p}\right)^{2k} \times \left\{ \frac{21}{32} \alpha_k \left(\frac{d}{r_p}\right)^{10} - \beta_k \left(\frac{d}{r_p}\right)^4 \right\} \right] \right) \quad (14)$$

The contribution of the dispersion forces to the adsorption enthalpy of carbon dioxide in silica is then $\xi_{\text{Dis-Int.}}^{\text{CO}_2} = 10.4 \text{ kJ/mol}$ for a cylindrical pore with a radius $r_p = 0.31 \text{ nm}$.

The adsorption enthalpy is approximately equal to the differential heat of adsorption, for a low coverage, then $\xi_{\text{Dis-Int.}}^{\text{CO}_2} \approx q_{\text{diff}}$; thereafter, because $q_{\text{iso}} = q_{\text{diff}} + RT$, we get finally that $q_{\text{iso}} = 12.8 \text{ kJ/mol}$. Because our experimental measurement of the isosteric heat of adsorption gives approximately equal results for all the silica, specifically, $q_{\text{iso}} = 28 \text{ kJ/mol}$, then it is 15 kJ/mol, which corresponds to other interactions. We know that the attraction of the quadrupole interaction is present here; however, this attraction normally does not contribute 15 kJ/mol, as was shown by a simulation process in silicalite.¹¹⁷ Besides, it has been also experimentally found the predominance of dispersion compared to electrostatic interactions in silicalite;¹⁰⁸ thereafter, another interaction must be present in the interaction between the silica surface and the carbon dioxide molecule. To get information about further contributions to the interaction between the silica surface and the carbon dioxide molecule, we will make a DRIFTS study.

3.2.3. Diffuse Reflectance Fourier Transform Spectrometry Study of the Adsorption of Carbon Dioxide in Silica. The adsorption interaction between the carbon dioxide molecule and the tested silica surfaces was also studied with the help of the DRIFTS spectra of carbon dioxide adsorbed on the tested silica surfaces at 300 K. In Figures 13–15 and Table 10 are reported the obtained data. These spectra show that the carbon dioxide molecule has some direct interactions with the surface of silica because of the presence of three peaks in the detected experimental absorption band. These peaks were evidenced by

fitting the experimental carbon dioxide infrared absorption band with the help of Lorentz functions.

The free carbon dioxide molecule belongs to the $D_{\infty h}$ group of symmetry, showing four fundamental vibration modes, that is, the symmetric stretching, $\nu_1(1338 \text{ cm}^{-1})$, the doubly degenerate bending vibration, ν_{2a} and ν_{2b} (667 cm^{-1}), and the asymmetric stretching vibration, ν_3 (2349 cm^{-1}).^{46–48} The ν_2 and ν_3 modes are infrared-active, whereas ν_1 is only Raman-active, in the free molecule.⁴⁷ However, when a carbon dioxide molecule interacts with a surface, it is no longer a free molecule, and its symmetry is lowered; as a result, the ν_1 mode becomes infrared-active, and a small band is observed,⁴³ whereas the other modes undergo moderate changes in wavenumber.^{45,49}

In Figures 13–15 and Table 10 is clearly evidenced that the asymmetric stretching vibration, ν_3 , of the adsorbed carbon dioxide molecule is observed at around 2340 cm^{-1} and corresponds to carbon dioxide physically adsorbed inside the silica micropores.¹¹³ The smaller band at about 2327 cm^{-1} is normally assigned to a combination band.^{45,48} It is possible to state that the absorption band observed at around 2340 cm^{-1} is the result of the attachment of the carbon dioxide molecule by dispersive and electrostatic forces to the adsorption space defined by the silica micropores. The adsorption process produces the confinement of the carbon dioxide molecule and, thereafter, the frequency shift and explains the band observed at around 2340 cm^{-1} and the combination band.

Additionally, another band is observed at around 2363 cm^{-1} . To explain this band, it is possible to state that, in the study of the adsorption of carbon dioxide on zeolites, the formation of weakly bonded adducts between the carbon dioxide molecule and the charge compensating cations, M^+ , is very well documented, as follows:^{37,43,45,49} $M^+ \cdots \delta^-O=C=O^\delta-$. Because, in acid zeolites, the proton acts as a compensating cation, then the formation of the following adduct $H^+ \cdots \delta^-O=C=O^\delta-$ is as well possible. Therefore, it is possible to conclude that the band found at around 2363 cm^{-1} corresponds to the antisymmetric stretching mode of carbon dioxide adsorbed on the

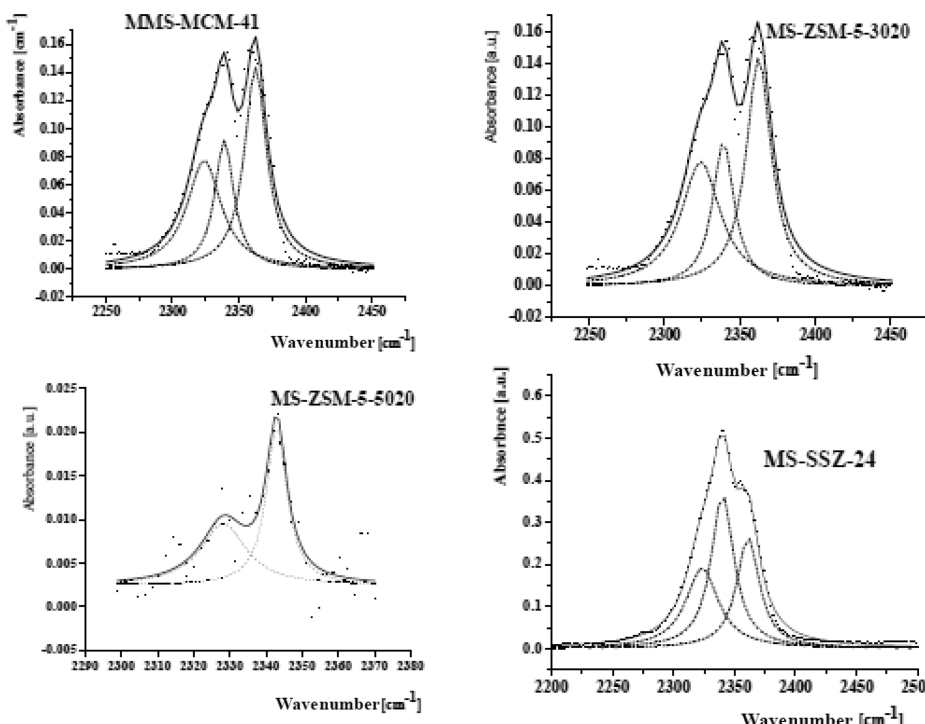


Figure 13. DRIFTS spectra of carbon dioxide adsorbed at 300 K on MMS-MCM-41, MS-ZSM-5-3020, MS-SSZ-24, and MS-ZSM-5-5020.

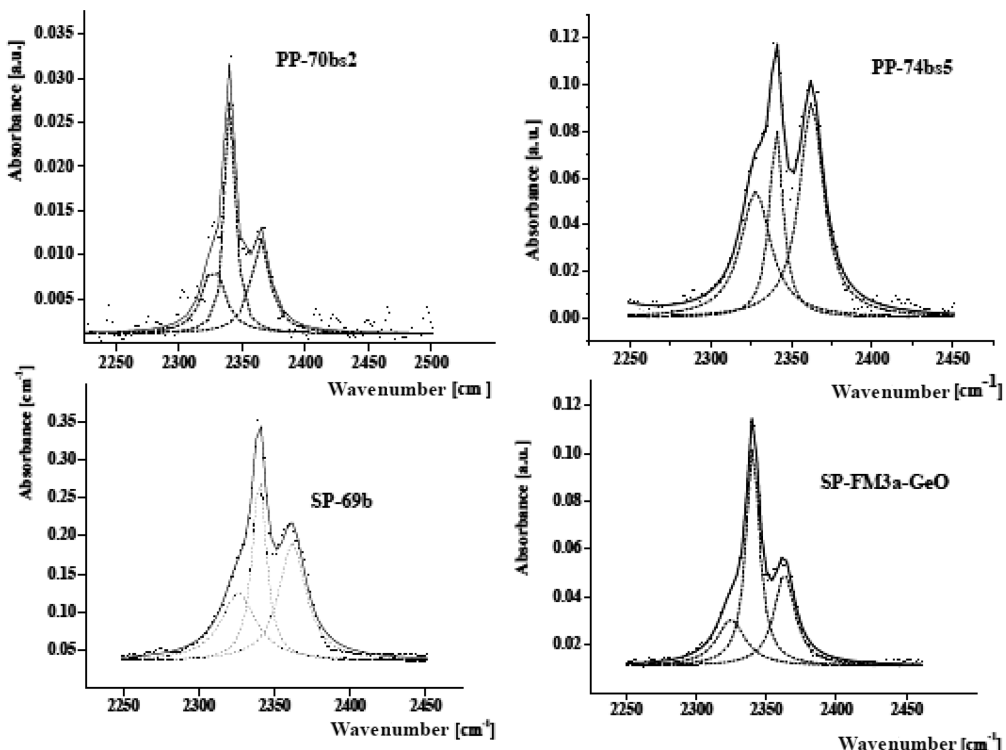


Figure 14. DRIFTS spectra of carbon dioxide adsorbed at 300 K on SP-69B, SP-FM3a-GeO, PP-70bs2, and PP-74bs5.

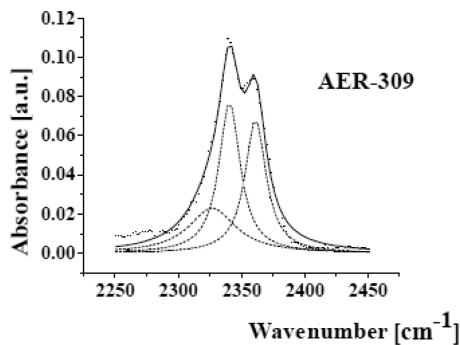


Figure 15. DRIFTS spectrum of carbon dioxide adsorbed at 300 K on AER-309.

TABLE 10: Resolved Peaks Positions

sample	x_c^1 [cm ⁻¹]	A_1 [%]	x_c^2 [cm ⁻¹]	A_2 [%]	x_c^3 [cm ⁻¹]	A_3 [%]
SP-69 ^a	2327	16.7	2341	49.3	2364	34.0
SP-80 ^a	2327	7.7	2338	53.8	2345	38.5
SP-FM3a-GeO ^a	2324	21.3	2340	22.4	2363	44.9
PP-74bs5 ^a	2327	32.7	2340	22.4	2362	44.9
PP-70bs2 ^a	2327	2.4	2341	18.9	2364	78.7
MMS-MCM-41 ^a	2328	34.2	2339	24.1	2362	41.7
MS-3020 ^a	2325	10.3	2339	40.8	2363	48.9
MS-SSZ-24 ^a	2324	30.7	2340	39.8	2361	29.5
AER-309 ^a	2326	26.1	2341	39.3	2361	34.6

^a SP means sphere packing silica xerogels, PP means particle packing silica xerogels, MS are molecular sieves, MMS is a mesoporous molecular sieve, and AER is an aerogel silica.

hydroxyl groups, forming a weakly bonded adduct as follows: $\text{H}^{\delta+} \cdots \delta^- \text{O}=\text{C}=\text{O}^{\delta-}$. This observation, as far as we know, is a new finding.

To further support this line of reasoning, it is possible to state that, during the study of the adsorption of carbon dioxide on zeolites with infrared spectroscopy,⁴³ this band is shifted, from 2346 cm⁻¹ for Cs-Y zeolite to 2356 cm⁻¹ for Li-Y, that is,

to higher frequencies for cations of smaller cationic radius. Because the proton has the smaller possible cationic radius, then the proposed interpretation of the observed band is reasonable. Another argument in favor of the formation of the previously described adduct is given during the adsorption of carbon dioxide on the MS-ZSM-5-5020, after 7 min of purging (see Figure 13). In the reported DRIFTS spectra, the intensities of the bands is reversed; that is, the band corresponding to the adduct is bigger than the band corresponding to the physically adsorbed carbon dioxide. This fact is possible because of the existence, as was previously shown (see Figure 10), of bridged OH groups in the MS-ZSM-5-5020 where the adsorption of the carbon dioxide molecule is stronger; consequently, the purge affects the intensity of this band less.

In Figure 16 are reported the DRIFTS difference spectra, in the OH region, of samples with carbon dioxide adsorbed and the same samples without carbon dioxide adsorbed. These spectra show, basically, a scatter of points; that is, it is difficult to identify real peaks. This fact indicates that carbon dioxide is not strongly enough adsorbed on the OH groups to affect the intensity of the OH bands, in our experimental conditions.

In short, we have commented in the previous section that the carbon dioxide molecule interacts with the silica surface through the dispersive and quadrupole interactions, which produces the fundamental adsorption interaction with the surface. However, the performed calculation of the contribution of the dispersive interactions and the analysis of the data reported in the literature indicated that at least one more weak interaction must be present. In agreement with this statement, the DRIFTS study indicated that the majority of carbon dioxide molecules interacting with the silica surface is physically adsorbed thorough dispersive and electrostatic interactions. However, additionally, the carbon dioxide molecules interact with the hydrogen included in the surface hydroxyl groups, forming a weakly bonded adduct as follows:⁴³ $\text{H}^{\delta+} \cdots \delta^- \text{O}=\text{C}=\text{O}^{\delta-}$.

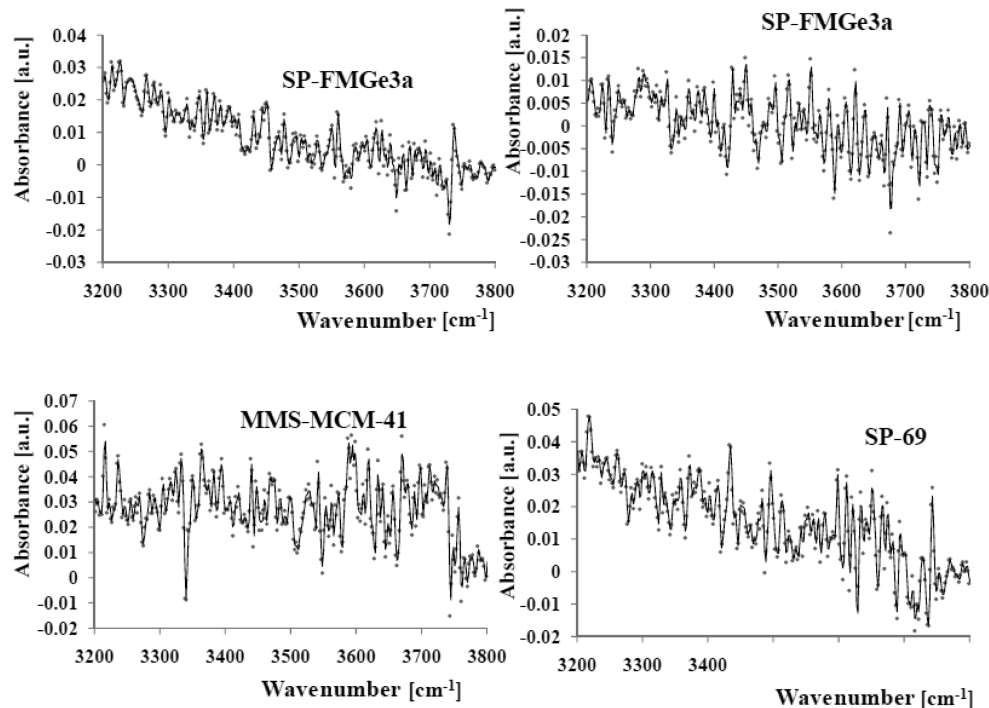


Figure 16. DRIFTS difference spectra, in the OH region, of samples with carbon dioxide adsorbed and without carbon dioxide adsorbed.

4. Conclusions

In the present paper, we have reported the study of carbon dioxide adsorption in properly characterized amorphous silica, particularly, three Stöber silicas, three extremely high specific surface area particle packing silica xerogels and two aerogels. In addition, other silica materials, such as MCM-41 and SSZ-24, two high Si/Al relation zeolites, that is, two ZSM-5 and one particularly high Si/Al relation zeolite, specifically, DAY, were also tested for comparison. These materials were examined with SEM, TGA, SAXS, DRIFTS, and adsorption of nitrogen at 77 K and carbon dioxide at 273 K. This approach is, by itself, innovative because normally these materials are individually studied.

It was shown that the sphere packing and particle packing silicas have a particular internal morphology that is composed of the secondary particles, evidenced by SEM, that is, aggregates composed of primary particles of around 15–20 nm for the SP silica and 7 nm for the PP silica. The reported microporosity is explained by the agglomeration of the primary particles to form the secondary particles, given that, in the agglomeration process, are created void spaces between the primary particles. To be precise, the SP, PP, and AER samples show micropore diameters in the range of $d^{\text{Mic}} = 0.56\text{--}0.59$ nm. These micropore diameters are similar to the opening of the 10 MR channel of the MFI framework, corresponding to the molecular sieves ZSM-5 and silicalite.

The specific surface area of the PP silicas, which was checked with a novel methodology, applying the TGA data, and one of the AER silica are 2–3 times bigger than those of the SP silicas and also 1.5 bigger than those of the MMS-MCM-41. These facts make the PP silica and one of the AER-909 samples very good materials for large specific surface area applications as adsorbents and catalyst supports. Specifically, the data reported show that the PP and AER samples exhibit a high specific surface area covered with hydroxyl groups, which are especially reactive with H₂O, and other polar molecules. This fact implies the potential application of these materials in the adsorption of

polar molecules. Additionally, the hydroxyl surface groups can be functionalized to modify the pore size, or influence the hydrophobicity of the pore wall. This change will permit the adsorption of nonpolar molecules. In addition, the impregnation of amines or the loading of alkali metals and other metals is as well feasible and reasonable on account of their high specific surface area and suitable surface chemistry. All these facts allow us to state that the PP and AER silicas could find wide application as adsorbents.

The reported carbon dioxide adsorption data allowed as well the measurement of the isosteric heat of adsorption with a single isotherm, applying an original methodology. The obtained data were compared with the calculated contribution of the dispersive interactions to the adsorption heat and the contribution of the quadrupole interaction was also qualitatively analyzed. This analysis indicated the existence of an additional interaction in the adsorption of carbon dioxide in silica.

To get information about the additional contributions to the whole interaction, a DRIFTS study was performed. In the obtained DRIFTS spectra was observed an absorption band at around 2340 cm⁻¹, which is a product of the confinement of the carbon dioxide molecule in the adsorption space formed by the silica micropores. In addition to the physically adsorbed carbon dioxide, it was also established by the careful interpretation of the DRIFT spectra of carbon dioxide adsorbed on silica that this molecule can participate in the role of proton acceptor; that is, the carbon dioxide molecules interact with the hydrogen included in the surface hydroxyl groups, forming a weakly bonded adduct as follows: H^{δ+}...^{δ-}O=C=O^{δ-}. This is a new finding as far as we know.

Acknowledgment. The authors acknowledge the financial support provided by the U.S. Department of Energy through the Massey Chair project at the University of Turabo. We also recognize the support of the National Science Foundation under the project CHE-0959334. We, as well, appreciate the collaboration of Bruker AXS Inc. in the training of our personnel in the operation of the D8 Advance System. The authors, as

well, gratefully thank our colleagues of the Department of Applied Physics of the Universidad Autonoma de Madrid for giving us the possibility to use the SEM facilities of the UAM. Finally, we also express our gratitude to Maria Cotto, Sheila Rosas, and Abraham Garcia for the help provided in the synthesis of the silica aerogels.

References and Notes

- (1) Young, D. M.; Crowell, A. D. *Physical Adsorption of Gases*; Butterworth: London, 1962.
- (2) Ross, S.; Olivier, J. P. *On Physical Adsorption*; Wiley: New York, 1964.
- (3) Gregg, S. J.; Sing, K. S. W. *Adsorption Surface Area and Porosity*; Academic Press: London, 1982.
- (4) Steele, W. A. *The Interaction of Gases with Solid Surfaces*; Pergamon Press: Oxford, U.K., 1974.
- (5) Sing, K. S. W.; Everett, D. H.; Haul, R. A. W.; Moscou, L.; Pirotti, R. A.; Rouquerol, J.; Siemieniewska, T. *Pure Appl. Chem.* **1985**, *57*, 603.
- (6) Rudzinski, W.; Everett, D. H. *Adsorption of Gases in Heterogeneous Surfaces*; Academic Press: London, 1992.
- (7) Rouquerol, F.; Rouquerol, J.; Sing, K. S. W. *Adsorption by Powder Porous Solids*; Academic Press: New York, 1999.
- (8) Thommes, M. In *Nanoporous Materials: Science and Engineering*; Lu, G. Q., Zhao, X. S., Eds.; Imperial College Press: London, 2004; p 317.
- (9) Roque-Malherbe, R. *Adsorption and Diffusion in Nanoporous Materials*; CRC Press: Boca Raton, FL, 2007.
- (10) Roque-Malherbe, R. *The Physical Chemistry of Materials: Energy and Environmental Applications*; CRC Press: Boca Raton, FL, 2010.
- (11) El Shafey, G. M. S. In *Adsorption on Silica Surfaces*; Papirer, E., Ed.; Marcel Dekker Inc.: New York, 2000; pp 34–62.
- (12) Brinker, C. J.; Scherer, G. W. *Sol-Gel Science*; Academic Press: New York, 1990.
- (13) Yong, Z.; Mata, V.; Rodrigues, A. E. *J. Chem. Eng. Data* **2000**, *45*, 1093.
- (14) Knöfel, C.; Martin, C.; Hornebecq, V.; Llewellyn, P. L. *J. Phys. Chem. C* **2009**, *113*, 21726.
- (15) Baxter, J.; Bian, Z.; Chen, G.; Danielson, D.; Dresselhaus, M. S.; Fedorov, A. G.; Fisher, T. S.; Jones, C. W.; Maginn, E.; Kortshagen, U.; Manthiram, A.; Nozik, A.; Rolison, D. R.; Sands, T.; Shi, L.; Sholl, D.; Wu, Y. *Energy Environ. Sci.* **2009**, *2*, 559.
- (16) Ho, M. T.; Allinson, G. W.; Wiley, D. E. *Ind. Eng. Chem. Res.* **2008**, *47*, 4883.
- (17) Huang, H. Y.; Yang, R. T.; Chinn, D.; Munson, C. L. *Ind. Eng. Chem. Res.* **2003**, *42*, 2427.
- (18) Dunne, J. A.; Rao, M.; Sircar, S.; Gorte, R. J.; Myers, A. L. *Langmuir* **1996**, *12*, 5896.
- (19) Bacsik, Z.; Atluri, R.; Garcia-Bennett, A. E.; Hedin, N. *Langmuir* **2010**, *26*, 10013.
- (20) Ruthven, D. M. *Principles of Adsorption and Adsorption Processes*; John Wiley and Sons: New York, 1984.
- (21) Ruthven, D. M.; Shamsuzzaman, F.; Knaebel, K. S. *Pressure Swing Adsorption*; John Wiley and Sons: New York, 1994.
- (22) Zhao, X.-X.; Xu, X.-L.; Sun, L.-B.; Zhang, L.-L.; Liu, X.-Q. *Energy Fuels* **2009**, *23*, 1534.
- (23) Deng, S. In *Encyclopedia of Chemical Processing*; Taylor and Francis: Boca Raton, FL, 2006; p 2825.
- (24) Leal, O.; Bolivar, C.; Ovalles, C.; Garcia, J.; Espidel, Y. *Inorg. Chim. Acta* **1995**, *240*, 183.
- (25) Rodriguez, I.; Iborra, S.; Corma, A.; Rey, F.; Jordà, J. *Chem. Commun.* **1999**, 593.
- (26) Chang, A. C. C.; Chuang, S. S. C.; Gray, M.; Soong, Y. *Energy Fuels* **2003**, *17*, 468.
- (27) Ma, X.; Wang, X.; Song, C. *J. Am. Chem. Soc.* **2009**, *131*, 5777.
- (28) Hiyoshi, N.; Yogo, K.; Yashima, T. *Microporous Mesoporous Mater.* **2005**, *84*, 357.
- (29) Srivastava, R.; Srinivas, D.; Ratnasamy, P. *J. Catal.* **2005**, *233*, 1.
- (30) Khatri, R. A.; Chuang, S. S. C.; Soong, Y.; Gray, M. *Energy Fuels* **2006**, *20*, 1514.
- (31) Srivastava, R.; Srinivas, D.; Ratnasamy, P. *Microporous Mesoporous Mater.* **2006**, *90*, 314.
- (32) Belmabkhout, Y.; De Weireld, G.; Sayari, A. *Langmuir* **2009**, *25*, 13275.
- (33) Shen, S. C.; Chen, X.; Kawi, S. *Langmuir* **2004**, *20*, 9130.
- (34) Hathaway, P. E.; Davis, M. E. *J. Catal.* **1989**, *116*, 263.
- (35) Kim, J. C.; Li, H.-X.; Chen, C.-Y.; Davis, M. E. *Microporous Mater.* **1994**, *2*, 413.
- (36) Bal, R.; Tope, B. B.; Das, T. K.; Hegde, S. G.; Sivasanker, S. J. *Catal.* **2001**, *204*, 358.
- (37) Jacobs, P. A.; Van Cauwelaert, F. M.; Vansant, E. F. *J. Chem. Soc., Faraday Trans.* **1973**, *69*, 2130.
- (38) Busca, G.; Lorenzelli, V. *Mater. Chem.* **1982**, *7*, 89.
- (39) Zecchina, A.; Otero Arean, C. *Chem. Soc. Rev.* **1996**, *25*, 187.
- (40) Lercher, G.; Gründling, C.; Eder-Mirth, G. *Catal. Today* **1996**, *27*, 353.
- (41) Lavalley, J. C. *Catal. Today* **1996**, *27*, 377.
- (42) Kazarian, S. G.; Vincent, M. F.; Bright, F. V.; Liotta, C. L.; Eckert, C. A. *J. Am. Chem. Soc.* **1996**, *118*, 1729.
- (43) Knozinger, H.; Huber, S. J. *J. Chem. Soc., Faraday Trans.* **1998**, *94*, 2047.
- (44) Garrone, E.; Fubini, B.; Bonelli, B.; Onida, B.; Otero Arean, C. *Phys. Chem. Chem. Phys.* **1999**, *1*, 513.
- (45) Bonelli, B.; Civalleri, B.; Fubini, B.; Ugliengo, P.; Otero Arean, C.; Garrone, E. *J. Phys. Chem. B* **2000**, *104*, 10978.
- (46) Nakamoto, K. *Infrared and Raman Spectra of Inorganic and Coordination Compounds: Part A: Theory and Applications in Inorganic Chemistry*; J. Wiley and Sons: New York, 1997; Vol. 1.
- (47) Bonelli, B.; Onida, B.; Fubini, B.; Otero-Arean, C.; Garrone, E. *Langmuir* **2000**, *16*, 4976.
- (48) Goodman, A. L.; Campus, L. M.; Schroeder, K. T. *Energy Fuels* **2005**, *19*, 471–476.
- (49) Llabres i Xamena, F. X.; Zecchina, A. *Phys. Chem. Chem. Phys.* **2002**, *4*, 1978.
- (50) Cazorla-Amoros, D.; Alcañiz-Monge, J.; Linares-Solano, A. *Langmuir* **1996**, *12*, 2820.
- (51) Cazorla-Amoros, D.; Alcañiz-Monge, J.; de la Casa-Lillo, M. A.; Linares-Solano, A. *Langmuir* **1998**, *14*, 4589.
- (52) *Powder Tech Note 35*; Quantachrome Instruments; Boynton Beach, FL.
- (53) Lowell, S.; Shields, J. E. *Powder Surface Area and Porosity*; Chapman & Hall: London, 1991.
- (54) Rege, S. U.; Yang, R. T. In *Adsorption. Theory, Modeling and Analysis*; Toth, J., Ed.; Marcel Dekker: New York, 2002; pp 175–210.
- (55) Yang, R. T. *Adsorbents. Fundamentals, and Applications*; J. Wiley and Sons: New York, 2003.
- (56) Rodriguez-Reinoso, F.; Linares-Solano, A. In *Chemistry and Physics of Carbon*; Thrower, P. A., Ed.; Marcel Dekker: New York, 1988; Vol. 21.
- (57) Stoeckli, H. F. *Russ. Chem. Bull.* **2001**, *50*, 2265.
- (58) Dubinin, M. M.; Stoeckli, H. F. *J. Colloid Interface Sci.* **1980**, *75*, 34.
- (59) Dubinin, M. M. *Prog. Surf. Membr. Sci.* **1975**, *9*, 1.
- (60) Dubinin, M. M. *American Chemical Society Symposium Series*; American Chemical Society: Washington DC, 1977; Vol. 40, p 1.
- (61) Bering, B. P.; Dubinin, M. M.; Serpinskii, V. V. *J. Colloid Interface Sci.* **1972**, *38*, 185.
- (62) Bering, B. P.; Serpinskii, V. V. *Izv. Akad. Nauk, SSSR, Ser. Xim.* **1974**, 2427.
- (63) Hutson, N. D.; Yang, R. T. *Adsorption* **1997**, *3*, 189.
- (64) Roque-Malherbe, R. *Microporous Mesoporous Mater.* **2000**, *41*, 227.
- (65) Stobe, W.; Fink, A.; Bohn, E. *J. Colloid Interface Sci.* **1968**, *26*, 62.
- (66) Iler, R. K. *The Chemistry of Silica*; J. Wiley and Sons: New York, 1979.
- (67) Pierre, A. C.; Pajonk, G. M. *Chem. Rev.* **2002**, *102*, 4243.
- (68) (a) Roque-Malherbe, R.; Marquez-Linares, F. *Mater. Sci. Semicond. Process* **2004**, *7*, 467. (b) Roque-Malherbe, R.; Marquez-Linares, F. *Surf. Interface Anal.* **2005**, *37*, 393.
- (69) Marquez-Linares, F.; Roque-Malherbe, R. *J. Nanosci. Nanotechnol.* **2006**, *6*, 1114.
- (70) Kresge, C. T.; Leonowicz, M. E.; Roth, W. J.; Vartuli, J. C.; Beck, J. S. *Nature* **1992**, *359*, 710.
- (71) Beck, J. S.; Vartuli, J. C.; Roth, W. J.; Leonowicz, M. E.; Kresge, C. T.; Schmitt, K. D.; Chu, C.T.-W.; Olson, D. H.; Sheppard, E. W.; McCullen, S. B.; Higgins, J. B.; Schlenker, J. L. *J. Am. Chem. Soc.* **1992**, *114*, 10834.
- (72) Barton, T. J.; Bull, L. M.; Klempner, G.; Loy, D. A.; McEnaney, B.; Misono, M.; Monson, P. A.; Pez, G.; Scherer, G. W.; Vartulli, J. C.; Yaghi, O. M. *Chem. Mater.* **1999**, *11*, 2633.
- (73) Davies, M. E. *Nature* **2002**, *417*, 813.
- (74) Lobo, R. F.; Pan, M.; Chan, I.; Li, H. X.; Medrud, R. C.; Zones, S. I.; Crozier, P. A.; Davis, M. E. *Science* **1993**, *262*, 1543.
- (75) Lobo, R. F.; Davis, M. E. *Microporous Mater.* **1994**, *3*, 61.
- (76) Lobo, R. F.; Davis, M. E. *J. Am. Chem. Soc.* **1995**, *117*, 3766.
- (77) Baerlocher, Ch.; Meier, W. M.; Olson, D. M. *Atlas of Zeolite Framework Types*, 5th ed.; Elsevier: Amsterdam, 2001.
- (78) *Making Silica Aerogels*; Environmental Energy Technologies Division, E.O. Lawrence Berkeley National Laboratory, University of California, U.S. Department of Energy, **2009**.
- (79) Albouy, P.-A.; Ayral, A. *Chem. Mater.* **2002**, *14*, 3391.

- (80) Selvam, P.; Bhatia, S. K.; Sonwane, Ch. G. *Ind. Eng. Chem. Res.* **2001**, *40*, 3237.
- (81) Muñiz, C.; Duconge, J.; Roque-Malherbe, R. *J. Colloid Interface Sci.* **2009**, *329*, 11.
- (82) Jones, B. *A Big Angle View of Small Angle Measurements SAXS Techniques*; BRUKER AXS: Madison, WI, www.bruker-axs.com.
- (83) Guinier, A. *X-Ray Diffraction in Crystals, Imperfect Crystals and Amorphous Bodies*; Dover Publications Inc.: New York, 1994.
- (84) Cullity, B. D.; Stock, S. R. *Elements of X-Ray Diffraction*, 3rd ed.; Prentice Hall: Upper Saddle River, NJ, 2001.
- (85) Roe, R. J. *Methods of X-ray and Neutron Scattering in Polymer Science*; Oxford University Press: New York, 2000.
- (86) Li, J.; Cookson, D. J.; Gerson, A. R. *Cryst. Growth Des.* **2008**, *8*, 1730.
- (87) Rieker, T. P.; Hindermann-Bischoff, M.; Ehrburger-Dolle, F. *Langmuir* **2000**, *16*, 5588.
- (88) Kammler, H. K.; Beauchage, G.; Mueller, R.; Pratsinis, S. E. *Langmuir* **2004**, *20*, 1915.
- (89) Boukari, H.; Lin, J. S.; Harris, M. T. *Chem. Mater.* **1997**, *9*, 2376.
- (90) Gommes, C.; Blacher, S.; Goderis, B.; Pirard, R.; Heinrichs, B.; Alie, Ch.; Pirard, J.-P. *J. Phys. Chem. B* **2004**, *108*, 8983.
- (91) Mascotto, S.; Wallacher, D.; Brandt, A.; Hauss, T.; Thommes, M.; Zickler, G. A.; Funari, S. S.; Timmann, A.; Smarsly, B. M. *Langmuir* **2009**, *25*, 12670.
- (92) Szekeres, M.; Toth, J.; Dekany, I. *Langmuir* **2002**, *18*, 2678.
- (93) Mueller, R.; Kammler, H. K.; Wegner, K.; Pratsinis, S. E. *Langmuir* **2003**, *19*, 160.
- (94) Jal, P. K.; Patel, S.; Mishra, B. K. *Talanta* **2004**, *62*, 1005.
- (95) Taylor, J. A. G.; Hockey, J. A.; Pethica, B. A. *Proc. Br. Ceram. Soc.* **1965**, *5*, 133.
- (96) Fripiat, J. J.; Uytterhoeven, J. *J. Phys. Chem.* **1965**, *66*, 800.
- (97) Vansant, E. F.; Van Der Voort, P.; Vrancken, K. C. *Characterization and Chemical Modification of the Silica Surface*; Elsevier: Amsterdam, 1995.
- (98) Gillis-D'Hamers, I. Ph.D. Thesis, University of Antwerp, Antwerp, Belgium, 1993.
- (99) Kisieliov, A. V.; Lygin, V. I. *Infrared Spectra of Surface Compounds*; J. Wiley and Sons: New York, 1975.
- (100) Zhuravlev, L. T. *Pure Appl. Chem.* **1989**, *61*, 1969.
- (101) Anedda, A.; Carbonaro, C. M.; Clemente, F.; Corpino, R.; Ricci, P. C. *J. Phys. Chem. B* **2003**, *107*, 13661.
- (102) Corma, A. *Chem. Rev.* **1995**, *95*, 559.
- (103) Roque-Malherbe, R.; Diaz-Castro, F. *J. Mol. Catal. A* **2008**, *280*, 194.
- (104) Barrer, R. M. *Zeolites and Clay Minerals as Sorbents and Molecular Sieves*; Academic Press: London, 1978.
- (105) Buckingham, A. D. *Proc. R. Soc. London, Ser. A* **1963**, *273*, 275.
- (106) Bai, R.; Deng, J.; Yang, R. T. *Langmuir* **2003**, *19*, 2776.
- (107) Barrer, R. M.; Gibbons, R. M. *Trans. Faraday Soc.* **1965**, *61*, 948.
- (108) Dunne, J. A.; Mariwala, R.; Rao, M.; Sircar, S.; Gorte, R. J.; Myers, A. L. *Langmuir* **1996**, *12*, 5888.
- (109) He, Y.; Seaton, N. A. *Langmuir* **2006**, *22*, 1150.
- (110) Derouane, E. G. In *Zeolites Microporous Solids: Synthesis, Structure and Reactivity*; Derouane, E. G., Lemos, F., Naccache, C., Ramos-Riveiro, F., Eds.; Kluwer Academic Publishers: Dordrecht, The Netherlands, 1992; pp 511–529.
- (111) Pinto, M. L.; Pires, J.; Carvalho, A. P.; de Carvalho, M. B. *J. Phys. Chem. B* **2006**, *110*, 250.
- (112) Yang, L.; Trafford, K.; Kresnawahjuesa, O.; Sepa, J.; Gorte, R. J.; White, D. *J. Phys. Chem. B* **2001**, *105*, 1935.
- (113) Goodman, A. L. *Energy Fuels* **2009**, *23*, 1101.
- (114) Horvath, G.; Kawazoe, K. *J. Chem. Eng. Jpn.* **1983**, *16*, 470.
- (115) Saito, A.; Foley, H. C. *AICHE J.* **1991**, *37*, 429.
- (116) Lide, D. R., Ed. *Handbook of Chemistry and Physics*, 83rd ed.; CRC Press: Boca Raton, FL, 2002–2003.
- (117) Goj, A.; Sholl, D. S.; Akten, E. D.; Kohen, D. *J. Phys. Chem. B* **2002**, *106*, 8367.

JP107754G